Surface segregation of primary glassy nanoparticles of $Fe_{90}Sc_{10}$ nanoglass

Chaomin Wang [a,b,*], Di Wang [a], Xiaoke Mu [a], Sunkulp Goel [c], Tao Feng [c], Yulia Ivanisenko [a], Horst Hahn [a,b,c], Herbert Gleiter [a,c]

[a] Institute of Nanotechnology, Karlsruhe Institute of Technology, 76344 Eggenstein-Leopoldshafen, Germany
[b] Joint Research Laboratory Nanomaterials, Technische Universität Darmstadt, Petersenstr. 32, 64287 Darmstadt, Germany
[c] Herbert Gleiter Institute of Nanoscience, Nanjing University of Science and Technology, 210094 Nanjing, China

ARTICLE INFO

Keywords:
Electron energy loss spectroscopy
Surface segregation
Glassy nanoparticles
Nanoglass
Interfaces

ABSTRACT

Electron energy loss spectroscopy (EELS) technique has been used to map the elemental distribution in $Fe_{90}Sc_{10}$ primary glassy nanoparticles (GNp) and in the corresponding nanoglass (NG) produced by consolidation of the GNp. Due to the effect of surface segregation, Fe has been identified to enrich at the surfaces of the primary GNp. This behavior was found to agree with the theoretical results calculated based on a monolayer model. In addition, the heterogeneous structure of $Fe_{90}Sc_{10}$ NG with Fe enriched interfaces have also been observed directly, which may be attributed to the surface segregation of the primary GNp.

1. Introduction

Adjusting the chemical composition at the surfaces or inter faces of alloys has been shown to be an effective approach to achieve desired properties of nanostructured materials [1 3].

In recent years, metallic glasses with nanometer sized struc tures, called nanoglasses, have attracted attention [2 4]. In fact, nanoglasses exhibit remarkable interface related properties such as the improved mechanical [4 7], biological [8], magnetic [9,10] and catalytic properties [11] in comparison to the corresponding melt quenched glasses of identical overall composition. Even though considerable research has been performed in order to study the mechanical, biological, magnetic properties of na noglasses, the knowledge of the atomic and the chemical structure of the interfaces between the glassy regions of nanoglasses is still rather limited.

In order to improve our understanding of the structure of the interfaces of nanoglasses, the chemical composition of isolated $Fe_{90}Sc_{10}$ primary GNp and the corresponding NG produced by consolidation of the GNp was investigated and is reported in this paper.

* Corresponding author at: Institute of Nanotechnology, Karlsruhe Institute of Technology, 76344 Eggenstein-Leopoldshafen, Germany.
E-mail address: chaomin.wang@partner.kit.edu (C. Wang).

2. Experiment

$Fe_{90}Sc_{10}$ NG was prepared by consolidation of the primary GNp produced by the inert gas condensation (IGC) method as described in previous work [4,9,12]. Specimens suitable for transmission electron microscopy (TEM) were prepared by attaching a carbon film (supported by a TEM grid) to the liquid nitrogen cooled cold finger of the IGC apparatus in order to collect the GNp directly. TEM specimens of $Fe_{90}Sc_{10}$ NG were prepared by focused ion beam (FIB). A FEI Titan 80 300 electron microscope operated at an accelerating voltage of 300 kV was used in the nanoprobe mode for Scanning TEM (STEM) imaging. The Fe and Sc elemental maps were acquired using a Gatan image filter (GIF) in energy filtered TEM (EFTEM) mode.

3. Results

Fig. 1(a) displays the STEM image of the primary GNp that were used to perform the elemental mapping. Fig. 1(b) and (c) shows the Fe and Sc maps for the primary GNp, respectively. By com paring Fig. 1(a) with Fig. 1(c), it may be seen that the diameters of the Sc rich regions are smaller than the primary particles, whereas the diameters of the Fe rich regions are as large as the primary particles (Fig. 1(b)). This observation indicates that the Sc con centration at the surfaces of the $Fe_{90}Sc_{10}$ primary GNp is too low to be detected. Fig. 1(d) was obtained by overlapping of Fig. 1(b) and (c) to confirm that Fe is concentrated on the surfaces of the GNp.

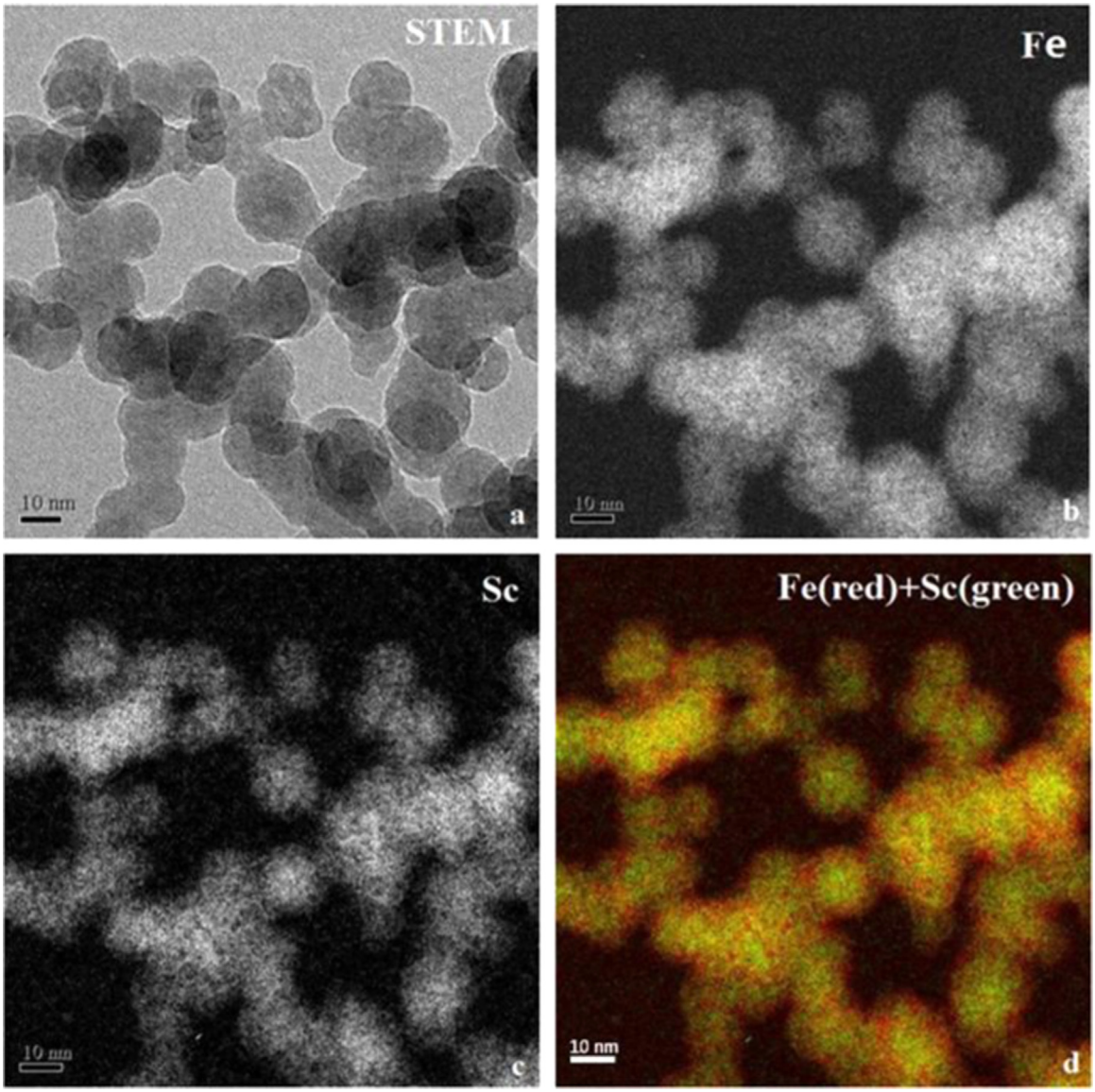

Fig. 1. EELS mapping of Fe and Sc in the primary $Fe_{90}Sc_{10}$ GNp. (a) STEM image, (b) Fe map, and (c) Sc map; (d) was obtained by overlapping (b) and (c); red color represent Fe, while green color represent Sc. (For interpretation of the references to color in this figure legend, the reader is referred to the web version of this article.)

Such segregation of the majority component to the free surfaces has also been found in $Sc_{75}Fe_{25}$ GNp, where Sc prefers to segregate to the surfaces [4].

EELS mapping of the $Fe_{90}Sc_{10}$ NG has been performed to con firm the segregation behavior reported above and to investigate the structure of $Fe_{90}Sc_{10}$ NG. In fact, the granular structure of the NG is visible in the STEM micrograph displayed in Fig. 2(a). EELS mapping of each components have been performed in the same manner as for the $Fe_{90}Sc_{10}$ GNp. By comparing the Fe and Sc maps, it may be noted that the Fe distribution is nearly uniform throughout the NG. Hence the boundaries between the glassy regions are almost invisible (Fig. 2(b)). In contrast, the distribution of Sc (Fig. 2(c)) is heterogeneous and shows up in the form of the nanometer sized "brighter dots" (indicated by the red arrows) connected by the darker areas. The "brighter dots" represent the interior of the glassy regions containing more Sc whereas the darker areas are the boundaries between the glassy regions with less Sc. The Fe enriched interfaces within $Fe_{90}Sc_{10}$ NG may be seen in Fig. 2(c). The heterogeneous structure of $Fe_{90}Sc_{10}$ NG is pre sented in Fig. 2(d) by superimposing of Fig. 2(b) and (c).

4. Discussion

In order to understand the origin of the surface segregation of Fe Sc GNp, a theoretical estimate of the chemical distribution based on a monolayer model has been carried out and was com pared with the experiment results.

Monolayer models are known to be applicable to estimate the surface composition of the liquid binary alloys as well as of solid solutions of binary alloys [13 17]. In monolayer models, solid so lutions of binary alloys are regarded as regular solutions. The surfaces of binary alloys are modeled as a monolayer and the compositional variations are assumed to be limited to the topmost monolayer. The driving force for surface segregation depends on two distinct contributions [14,15,18]: One contribution results from the different surface energies of the two pure components. The second contribution depends on the heat of mixing, ΔH_{mix}, of both components, or the degree of negativity of ΔH_{mix}. Since binary metallic glasses (MG) are metastable frozen liquid alloys [19], their atomic structures may be approximated by the struc tures of the corresponding molten state [20]. In other words, they could be treated as solid solution of binary alloys fitted to the

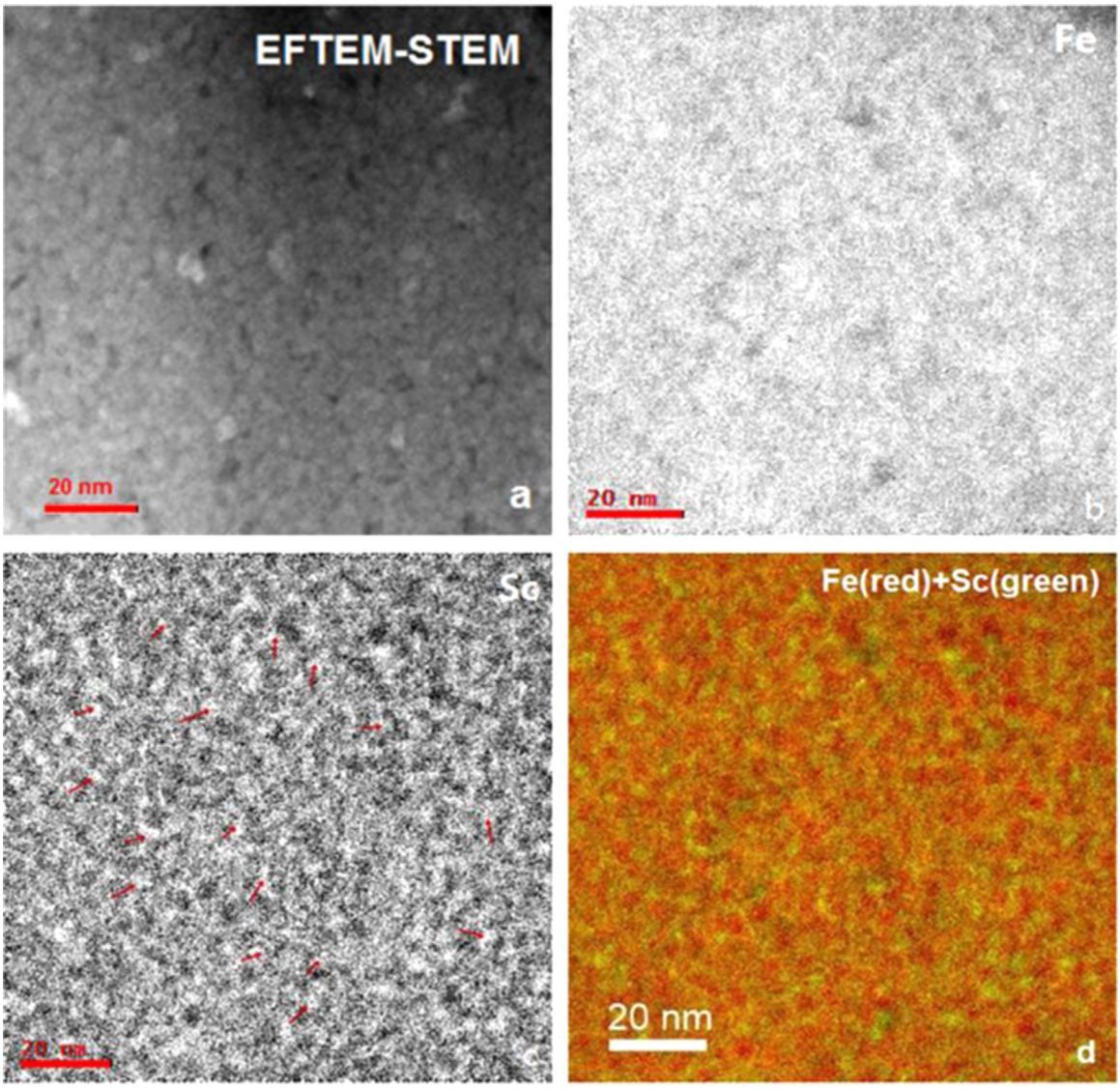

Fig. 2. EELS mapping of Fe and Sc from the $Fe_{90}Sc_{10}$ NG. (a) STEM image, (b) Fe map, and (c) Sc map; the "bright dots" indicated by the red arrows are the Sc richer cores; (d) was obtained by overlapping (b) and (c); red color represent Fe, while green color represent Sc. (For interpretation of the references to color in this figure legend, the reader is referred to the web version of this article.)

monolayer model.

The equation derived from the monolayer model may be written in the following form [17]:

$$\frac{X_1^i}{X_1^S} = \frac{X_2^i}{X_2^S} \exp\left(\frac{S_1 - S_2}{RT}\right) f(W) \tag{1}$$

X_1^s and X_1^i are the molar fraction of component "1" on the surface and the interior of the binary liquid alloy, respectively. Since, $X_1^S + X_2^S = 1$, $X_1^i + X_2^i = 1$. S_1 and S_2 are the molar pure component surface energies of 1 and 2, respectively. R is the gas constant, T is the absolute temperature. $f(W)$ is the regular solution function for the heat of mixing components and can be derived by equation as:

$$f(W) = \exp\left\{\frac{W(l+m)}{RT}\left[\left(X_1^i\right)^2 - \left(X_2^i\right)^2\right] + \frac{Wl}{RT}\left[\left(X_2^S\right)^2 - \left(X_1^S\right)^2\right]\right\} \tag{2}$$

Here, W is defined as $W = z(E_{12} - (E_{11}+E_{22})/2)$, and z is the total number of next neighbor contacts. E_{11}, E_{22} and E_{12} are the bond energies, where, E_{11} can be defined as the bond energy between per mole atoms of component 1 and similarly E_{22} and E_{12}. For ideal solution, $W=0$ and $f(W)=1$. l and m denote the fractions of the total next neighbor contacts made by an atom with its own layer and neighboring next layer. Accordingly, the total number of next neighbor contacts of the interior atom is $(l+2m)z$, while that of the surface layer is $(l+m)z$, and $(l+2m)=1$[13].

The molar surface energies of pure Fe and pure Sc can be calculated based on the relationship between the surface energy and the heat of sublimation as $S = 0.16\ \Delta H^{sub}$ [16]. The heat of sublimation for Fe and Sc are taken from the literature as $\Delta H_{Fe}^{sub} = 415.50$ kj mol^{-1} [21] and $\Delta H_{Sc}^{sub} = 381.70$ kj mol^{-1} [22]. The obtained value after calculating the surface energy of Fe and Sc is $S_{Fe} = 66.48$ kj mol^{-1} and $S_{Sc} = 61.07$ kj mol^{-1}, respectively.

W can be derived from the heat of mixing of Fe with Sc above as $W = \Delta H^{mix}/X_{Fe}{}^i X_{Sc}{}^i$ [23], where $\Delta H^{mix} =$ 11.28 kj mol^{-1} [24]. The choice of l and m values depends on the atomic packing manners [25]. In the glassy state, the atoms are treated as randomly distributed in a nearly closed packed structure [26]. Accordingly $l=0.5$, and $m=0.25$ are always chosen for the binary MG and liquid alloys [13,25]. However, due to the relaxation effect, it was

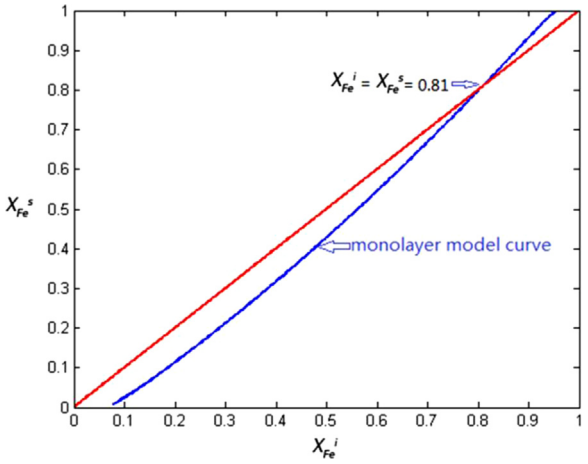

Fig. 3. Plot obtained by calculating the Fe composition on the surface verses Fe composition on the interior of Fe-Sc MG based on the monolayer model. (For interpretation of the references to color in this figure, the reader is referred to the web version of this article.)

proposed to use $l=0.75$ instead of $l=0.5$ [27]. Furthermore, according to radial distribution function (RDF) of $Fe_{90}Sc_{10}$ NG [28], the number of next neighbor contacts of Fe at the interfaces and interior cores are 9.1 and 10.5, respectively. Thus, the values of $l=0.75$ and $m=0.125$ could be calculated from:

$$\left.\begin{aligned}(l+m)z &= 9.1\\ (l+2m)z &= z = 10.5\end{aligned}\right\} \quad (3)$$

After substituting the values in Eq. (1) and taking $X_1^{\,i}=X_{Fe}^{\,i}$ as independent variable and $X_1^{\,s}=X_{Fe}^{\,s}$ dependent variable, the plotted results are shown in Fig. 3.

As may be seen from Fig. 3 the red line represents no surface segregation, i.e., $X_{Fe}^{\,s}=X_{Fe}^{\,i}$. The theoretical values (blue curve) characterized by the Fe concentration below the intersection ($X_{Fe}^{\,s}=X_{Fe}^{\,i}=0.81$) imply that the Fe atoms accumulate in the interior of the Fe Sc MG. The opposite applies to Fe Sc MG with Fe concentration above the intersection. In these MG, the Fe is enhanced in the surface regions. Obviously, in Sc rich MG, segregation of the majority component happens for all compositions. However, in Fe rich MG, the majority component Fe starts to segregate only when Fe concentration above the intersection. Clearly, this result is consistent with the experimental observations for $Sc_{75}Fe_{25}$ and $Fe_{90}Sc_{10}$ GNp, i.e. Sc segregate to the surfaces of $Sc_{75}Fe_{25}$ GNp while Fe prefer to segregate to the surfaces of $Fe_{90}Sc_{10}$ GNp. And this result is also consistent with recent molecular dynamics simulations that the majority component would like to segregate to the surfaces of the vapor deposited GNp [29].

In conclusion, the tendency of the blue curve could be simply explained as the combined effects of the two kinds of driving forces for surface segregation. Since, Sc has lower surface energy, the reduction of the surface energy provides the driving force for the segregation of the Sc to the surfaces. However, the driving force resulting from the reduced energy of the Fe Sc bond will provide a driving force for moving the minority components into interior of the GNp. Therefore, by changing the composition of Fe Sc MG, these two driving force are balanced against each other and result in the experimentally observed different surface segregation for different chemical compositions.

Since the Fe Sc nanoglasses were produced by consolidation of primary GNp, the surface segregation effect of the primary GNp controls the chemical composition of the interfaces of the as consolidated nanoglasses.

5. Summary

Surface segregation of Fe was observed by means of electron energy loss spectroscopy to occur in $Fe_{90}Sc_{10}$ glassy nanoparticles. This surface segregation was found to result in a chemically heterogeneous structure of $Fe_{90}Sc_{10}$ nanoglass. The results of a theoretical study by means of a monolayer model of the surface segregation of $Fe_{90}Sc_{10}$ glassy nanoparticles were found to agree with the experimentally observed segregation effects.

Acknowledgement

One of us (H.H.) gratefully acknowledges the partial financial support of this work by the Deutsche Forschungsgemeinschaft under the Priority Programme SPP 1594 “Topological Engineering of Ultra Strong Glasses”. C.M.W gratefully acknowledges support from China Scholarship Council (CSC).

References

[1] S. Zafeiratos, S. Piccinin, D. Teschner, Alloys in catalysis: phase separation and surface segregation phenomena in response to the reactive environment, Catal. Sci. Technol. 2 (2012) 1787–1801.
[2] H. Gleiter, Nanoglasses: a new kind of noncrystalline materials,, Beilstein J. Nanotechnol. 4 (2013) 517–533.
[3] H. Gleiter, T. Schimmel, H. Hahn, Nanostructured solids - from nano-glasses to quantum transistors, Nano Today 9 (2014) 17–68.
[4] J.X. Fang, U. Vainio, W. Puff, R. Wurschum, X.L. Wang, D. Wang, M. Ghafari, F. Jiang, J. Sun, H. Hahn, H. Gleiter, Atomic structure and structural stability of $Sc_{75}Fe_{25}$ nanoglasses, Nano Lett. 12 (2012) 458–463.
[5] X.L. Wang, F. Jiang, H. Hahn, J. Li, H. Gleiter, J. Sun, J.X. Fang, Plasticity of a scandium-based nanoglass, Scr. Mater. 98 (2015) 40–43.
[6] X.L. Wang, F. Jiang, H. Hahn, J. Li, H. Gleiter, J. Sun, J.X. Fang, Sample size effects on strength and deformation mechanism of $Sc_{75}Fe_{25}$ nanoglass and metallic glass, Scr. Mater. 116 (2016) 95–99.
[7] N. Chen, D.V. Louzguine-Luzgin, G.Q. Xie, P. Sharma, J.H. Perepezko, M. Esashi, A.R. Yavari, A. Inoue, Structural investigation and mechanical properties of a representative of a new class of materials: nanograined metallic glasses, Nanotechnology 24 (2013) 045610.
[8] N. Chen, X.T. Shi, R. Witte, K.S. Nakayama, K. Ohmura, H.K. Wu, A. Takeuchi, H. Hahn, M. Esashi, H. Gleiter, A. Inoue, D.V. Louzguine, A novel Ti-based nanoglass composite with submicron-nanometer-sized hierarchical structures to modulate osteoblast behaviors, J. Mater. Chem. B 1 (2013) 2568–2574.
[9] R. Witte, T. Feng, J.X. Fang, A. Fischer, M. Ghafari, R. Kruk, R.A. Brand, D. Wang, H. Hahn, H. Gleiter, Evidence for enhanced ferromagnetism in an iron-based nanoglass, Appl. Phys. Lett. 103 (2013).
[10] M. Ghafari, H. Hahn, H. Gleiter, Y. Sakurai, M. Itou, S. Kamali, Evidence of itinerant magnetism in a metallic nanoglass, Appl. Phys. Lett. 101 (2012).
[11] N. Chen, R. Frank, N. Asao, D. Louzguine-Luzgin, P. Sharma, J. Wang, G. Xie, Y. Ishikawa, N. Hatakeyama, Y. Lin, Formation and properties of Au-based nanograined metallic glasses, Acta Mater. 59 (2011) 6433–6440.
[12] T. Feng, D. Wang, C.M. Wang, N. Chen, H. Hahn, H. Gleiter, Generating metallic amorphous core–shell nanoparticles by a solid-state amorphization process, Part. Part. Syst. Charact. 33 (2016) 82–88.
[13] E. Guggenheim, Statistical thermodynamics of the surface of a regular solution, Trans. Faraday Soc. 41 (1945) 150–156.
[14] M.J. Osborne, D.J. Lacks, Surface segregation in liquid mixtures with strong interspecies attraction, Phys. Rev. E 70 (2004) 010501.
[15] S. Saw, S. Kamil, C. Dasgupta, Spatial modulation of the composition of a binary liquid near a repulsive wall, Phys. Rev. E 91 (2015) 052406.
[16] S. Overbury, P. Bertrand, G. Somorjai, Surface composition of binary systems. Prediction of surface phase diagrams of solid solutions, Chem. Rev. 75 (1975) 547–560.
[17] R. Defay, I. Prigogine, A. Bellemans, D.H. Everett, Surface Tension and Adsorption, Wiley, New York, 1966.
[18] P. Wynblatt, D. Chatain, Anisotropy of segregation at grain boundaries and surfaces, Metall. Mater. Trans. A 37A (2006) 2595–2620.
[19] W. Kauzmann, The nature of the glassy state and the behavior of liquids at low temperatures, Chem. Rev. 43 (1948) 219–256.
[20] J. Dyre, Glasses: heirs of liquid treasures, Nat. Mater. 3 (2004) 749–750.
[21] P.D. Desai, Thermodynamic properties of iron and silicon, J. Phys. Chem. Ref. Data 15 (1986) 967–983.
[22] O.H. Krikorian, The vapor pressure of scandium metal, J. Phys. Chem. 67 (1963) 1586–1589.
[23] R.A. Swalin, Thermodynamics of Solids, 2nd ed., Wiley, New York, 1972.
[24] F.R. de Boer, R. Boom, W.C.M. Mattens, A.R. Miedema, A.K. Niessen, Cohesion in Metals: Transition Metal Alloys, Elsevier Science, New York, 1988.

[25] O.E. Awe, A. Onifade, Effects of surface coordination of atoms on the surface properties of some liquid binary alloys, Phys. Chem. Liq. 50 (2012) 579–595.
[26] J.D. Bernal, Geometry of the structure of monatomic liquids, Nature 185 (1960) 68–70.
[27] T. Hoar, D. Melford, The surface tension of binary liquid mixtures: lead+tin and lead+indium alloys, Trans. Faraday Soc. 53 (1957) 315–326.
[28] M. Ghafari, S. Kohara, H. Hahn, H. Gleiter, T. Feng, R. Witte, S. Kamali, Struc-tural investigations of interfaces in $Fe_{90}Sc_{10}$ nanoglasses using high-energy x-ray diffraction, Appl. Phys. Lett. 100 (2012).
[29] D. Danilov, H. Hahn, H. Gleiter, W. Wenzel, Mechanisms of Nanoglass Ultra-stability, ACS Nano 10 (2016) 3241–3247.